WILEY InterScience® DISCOVER SOMETHING GREAT

PROTEINS STRUCTURE ■ FUNCTION ■ BIOINFORMATICS

# Conformational flexibility in mammalian 15S-lipoxygenase: Reinterpretation of the crystallographic data

**Jongkeun Choi,[1] Jae Kyung Chon,[2] Sangsoo Kim,[3] and Whanchul Shin[1,2]***

[1] Department of Chemistry, Seoul National University, Seoul, Korea

[2] Program in Bioinformatics, Seoul National University, Seoul, Korea

[3] Department of Bioinformatics, Soongsil University, Seoul, Korea

*ABSTRACT*

***Lipoxygenases (LOXs) are a family of nonheme iron dioxygenases that catalyze the regioselective and stereospecific hydroperoxidation of polyunsaturated fatty acids, and are involved in a variety of inflammatory diseases and cancers. The crystal structure of rabbit 15S-LOX1 that was reported by Gillmor et al. in 1997 has played key roles for understanding the properties of mammalian LOXs. In this structure, three segments, including 12 residues in the superficial α2 helix, are absent and have usually been described as "disordered." By reinterpreting the original crystallographic data we were able to elucidate two different conformations of the molecule, both having well ordered α2 helices. Surprisingly, one molecule contained an inhibitor and the other did not, thereby adopting a closed and an open form, respectively. They differed in the conformation of the segments that were absent in the original structure, which is highlighted by a 12 Å movement of α2. Consequently, they showed a difference in the size and shape of the substrate-binding cavity. The new model should provide new insight into the catalytic mechanism involving induced conformational change of the binding pocket. It may also be helpful for the structure-based design of LOX inhibitors.***

Proteins 2008; 70:1023–1032.


*Key words: crystal structure; ligand-induced conformational change; arachidonate binding mode; crystal twinning; pseudo symmetry.*

## INTRODUCTION

Lipoxygenases (LOXs) are nonheme iron dioxygenases that catalyze the regioselective and stereospecific hydroperoxidation of polyunsaturated fatty acids.[1] LOXs are found in a large variety of organisms, such as bacteria, plants, and mammals.[2–4] In plants, LOXs are involved in germination and senescence and their typical substrate is linoleic acid or α-linolenic acid.[4] In mammals, LOXs together with cyclooxygenases are key enzymes in the arachidonic acid cascade.[5] LOXs produce hydroperoxyeicosatetraenoic acids, precursors of leukotrienes and lipoxins that have been implicated as critical signaling molecules in a variety of inflammatory diseases and cancers.[6–9]

The crystal structures of soybean LOX-L1[10] and LOX-L3,[11] rabbit 15*S*-LOX1,[12] and coral 8*R*-LOX[13] have been elucidated thus far and helped understanding the properties of LOXs at the molecular level. Several structures of soybean LOX in complex with its product or inhibitor are also known.[14–18] There are significant differences in size, sequence, and substrate preference between the plant and animal LOXs, but the overall fold and geometry of the nonheme iron-binding site are conserved.[19,20] All LOXs are folded in a two-domain structure that is composed of a smaller N-terminal β-barrel and a larger α-helical catalytic domain. The nonheme iron essential for activity is positioned deep in a large cavity that accommodates the substrate. The regio- and stereospecificities of the various LOX isozymes are believed to be determined by the shape and depth of the cavity as well as the binding orientation of the substrate in the cavity.[21–23]

The crystal structure of 15*S*-LOX1 in complex with inhibitor was reported by Gillmor *et al.*[12] Ever since, it has served key roles in understanding the specificities of mammalian LOXs as well as designing structure-based inhibitors.[7,24,25] This structure was determined in the trigonal space group R32 at 2.4 Å resolution. In the PDB model (1lox), the atomic coordinates for many residues (177−188, 210−211, and 601−602) are not available and a superficial α-helix (α2) exists as disconnected even though residues 177−188 could have been modeled into it bridging the gap. According to the original article, "There is no density for surface residues 210−211 and 601−602. The density for residues 177−188 is 'ambiguous'

Grant sponsor: Center for Biological Modulators, The 21st Century Frontier R&D Program, Ministry of Science and Technology (MOST), Korea; Grant number: CBM2-B512-001-1-0-0.
*Correspondence to: Whanchul Shin, Department of Chemistry, Seoul National University, Seoul 151-742, Korea. E-mail: nswcshin@plaza.snu.ac.kr
Received 31 October 2006; Revised 10 March 2007; Accepted 22 March 2007
Published online 10 September 2007 in Wiley InterScience (www.interscience.wiley.com).
DOI: 10.1002/prot.21590

due to the nearby presence of a twofold crystallographic symmetry operator." In subsequent articles citing this structure, this α-helix has been described as "disordered," although it is very unlikely that a segment within a long α-helix is disordered.

Recently, Oldham *et al.* compared the structure of 8*R*-LOX with that of 15*S*-LOX1 and noted some significant discrepancies.[13] They pointed out that the crystal packing constraints were violated in the "disordered" helical segment in 15*S*-LOX1 structure. We found that the two helices related by a crystallographic twofold axis on the diagonal between the *a* and *b* axes collided with each other [Fig. 1(a)], while the electron density map showed a contiguous density accommodating both ends of the helix [Fig. 1(b)]. This suggests that residues 177−187 were absent not because they were disordered but because they could not be modeled within the constraints of crystal packing. As the original model cannot be compatible with the crystal packing constraint, we have sought out alternative models. In this study, we reinterpreted the original crystallographic data using the R3 twin model and obtained the complete structure of two independent molecules that partly assumed different conformations. The new model is sound crystallographically in that there is no crystal packing problem and at the same time the "disordered" α2 helix is well resolved. It should provide new insight into the catalytic mechanism involving induced conformational change of the binding pocket. It may also be helpful for the structure-based design of LOX inhibitors.

## METHODS

### Crystallographic analysis

The electron density map calculated with the structure factors and coordinates downloaded from PDB displayed not only a contiguous density connecting the "disordered" helix but also a chunk of unaccounted density ~10 Å away from it [Fig. 1(b)]. The size and shape of the latter, when properly refined, might have been able to accommodate a few turns of α-helix. It appeared that we could build two kinds of conformation of the helix into these densities. In the space group R32 where the original structure had been solved, a crystallographic twofold axis passed through these densities. If two molecules of the same kind of conformation were to pack around the twofold axis, the helix would bump into each other. Thus, one conformer had to pack with the other conformer to satisfy crystal packing constraints. We inferred that this kind of packing could be achieved by employing two alternative assumptions (see Appendix for details). One (R32 disorder model) was that a protein molecule was disordered in two conformations in R32. The other (R3 twin model) was that the two protein molecules were related by pseudo-twofold symmetry rather than crystallographic one, which implied that the space group was shifted into R3. In this case, the crystal should have been twinned according to a statistical test (see Appendix for details). Both models would be virtually indistinguishable in terms of the final refinement statistics. However, we preferred to use the R3 twin model as it was easier to perform model building and refinement than with the R32 disorder model. Refinement was carried out using the twin option in the CNS package.[26] Relieving the crystallographic twofold symmetry allowed us to model and refine two protein molecules that significantly differed in the α2 helix; the helix runs through the "disordered" region in one molecule and through the density ~10 Å away from it in the other molecule.

### Model building and refinement

The initial R3 dimer model of 15*S*-LOX1 was made from the PDB coordinates: ($x$, $y$, $z$) for one molecule and ($1/3 + y$, $2/3 + x$, $2/3 - z$) obtained by twin operation for the other. In the R32 structure, the coordinates for 15 residues (177−187, 210−211, and 601−602) were absent.[12] In addition, 19 residues (Lys21, Lys45, Arg66, Lys68, Glu147, Lys157, Asp174, Ser189, Ser191, Leu192, Asn193, Lys199, Ile207, Arg212, Ser327, Gln596, Gln599, Pro600, and Ile603) were modeled as alanines; two thirds of them are near the missing residues.

The model was built using the program O.[27] Refinement was carried out using the twin option in CNS, typically with positional refinement, followed by simulated annealing to 3000 K, and finally, individual B-factor refinement.[26] Manual rebuilding was carried out between each run with $\sigma_A$-weighted, $2F_o - F_c$ maps. For the $R_{free}$ calculation, 10% of the data were randomly selected and set aside. Even in the initial electron density map, residues in the two α2 helices could be easily fitted into the densities. However, further model building and refinement had to be performed meticulously and numerous iterations were necessary to trace several chains, especially, those connected to α2. As the model building proceeded, the symmetric relationship between the two independent molecules started to break down. Eventually, their structures became different assuming an "open" and a "closed" form, respectively; the former is more or less similar to the original R32 structure while the latter is substantially dissimilar.

The electron density for the inhibitor was found only in the closed form. The atomic positions and B-factors of the inhibitor were refined. Water molecules were picked up from the $2F_o - F_c$ and $F_o - F_c$ difference maps on the basis of the peak heights and distance criteria, and were retained only when the B-factor after refinement was below 80 Å$^2$. Noncrystallographic symmetry restraints were not applied throughout the structure refinement. The final $R$ factor was 0.193 and $R_{free}$ 0.230. The $R$ factor could have been lowered but only at

 DOI 10.1002/prot

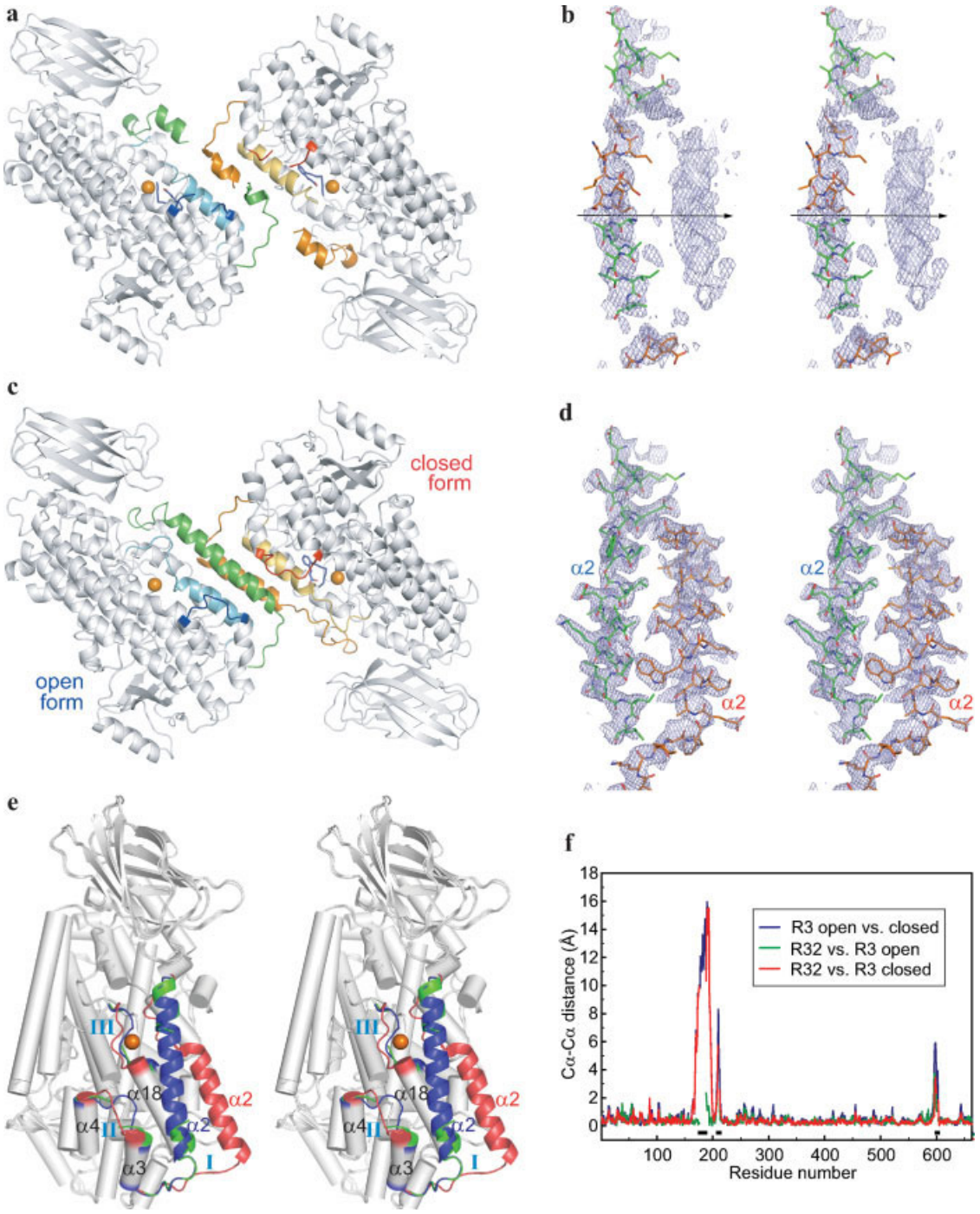


**Figure 1**

*Comparison of the original R32 and new R3 structures of 15S-LOX1. (**a**) Ribbon diagram of the original R32 structure showing a dimer related by crystallographic twofold symmetry with a viewing direction along the twofold axis. The regions near the missing residues are colored. The inhibitor is depicted as a stick model in blue and the catalytic iron as a sphere in orange. (**b**) Stereoview of the $2F_o - F_c$ map near α2 in R32, contoured at 1.0 σ. The disconnected α2 helix and its symmetry-related mate are depicted as stick models with C—C bonds in green and orange, respectively. A crystallographic twofold axis in the diagonal between the a and b axes in R32 is depicted as an arrow in black. (**c**) Ribbon diagram of the new R3 structure showing two independent molecules related by pseudo-twofold symmetry. The regions that significantly differ in the open and closed forms are colored. The inhibitor is depicted as a stick model in blue and the catalytic iron as a sphere in orange. (**d**) Stereoview of the $2F_o - F_c$ map near the α2 helices in R3, contoured at 1.0 σ. The α2 helices of the open and closed forms are depicted as stick models with C—C bonds in green and orange, respectively. (**e**) Superposed structures (in stereoview) of the R32 model (green) and the R3 open (blue) and closed (red) forms. Only those regions where the structures are significantly different are colored. Labels I, II, and III represent the segments that show large differences between the R3 open and closed forms. (**f**) Plot for the Cα···Cα distance versus residue number. Short thick bars in black above the abscissa denote the residues missing in the R32 model.*

**Table I**
*Crystallographic Statistics*

| | |
|---|---|
| X-ray data | |
| Space group | *R*3 (*R*32)[a] |
| Cell parameters, *a*, *b*, *c* (Å) | 198.9, 198.9, 136.1 |
| Resolution (Å) | 16–2.4 |
| Reflections, unique | 76159[b] (39132) |
| Completeness (%) | 97.3 (97.9) |
| Refinement | |
| Number of residues | 1324 (649) |
| Number of water molecules | 219 (94) |
| Number of ligand | 1 (1) |
| *R* (%)[c] | 19.3 (19.8) |
| $R_{free}$ (%) | 23.0 (24.7) |
| *rms* bond length (Å) | 0.01 (0.01) |
| *rms* bond angles (°) | 1.45 (1.53) |
| Average B-factor (Å$^2$) | 46.8 (48.6) |
| Main chain atoms | 46.7 (47.6) |
| Side chain atoms | 46.9 (49.6) |
| Ligand atoms | 71.4 (73.0) |
| Water molecules | 26.3 (39.4) |
| Ramachandran plot[d] | |
| Most favored (%) | 87.2 (87.5) |
| Additionally allowed (%) | 12.5 (12.1) |
| Generously allowed (%) | 0.3 (0.4) |
| Disallowed (%) | 0.0 (0.0) |

[a]The values for the original *R*32 structure are in parentheses.
[b]The *R*3 data contains the $|F_o(hkl)|$ reflections downloaded from PDB and twin-related $|F_o(kh-l)|$'s generated by equating $|F_o(kh-l)|$ to $|F_o(hkl)|$ using the program SFTOOLS in the CCP4 package with an option to generate the symmetry related reflections.[28]
[c]$R = \sum||F_{obs}| - |F_{calc}||/\sum|F_{obs}|$. $R_{free}$ is the same as *R*, but for a randomly chosen 10% of reflections that were not used in structure refinement.
[d]Statistics are for the nonglycine, nonproline, and non-N- or non-C-terminal residues.

the expense of the quality of the model and $R_{free}$ value. In the final density map, there was no ambiguous segment in the protein backbone. The side chains of 11 residues (out of 1324), mostly on the protein surface, were disordered or ambiguous because of weak densities, but were modeled considering the interactions with their environments. The residues in several segments of the N-terminal β-barrel and the chains connected to α2 had large B-factors; notably, average B-factors for residues 11–47, 52–56, 66–75, 169–172, 205–214, and 595–602 in the open form and residues 13–34, 40–45, 52–58, 64–75, 84–92, 126–129, 163–177, 189–214, and 595–604 in the closed form were larger than 60 Å$^2$. A summary of refinement statistics is shown in Table I. The stereochemical analysis was performed using the program PROCHECK.[29] The atomic coordinates have been deposited in the PDB under accession code 2P0M. As we used the twin model, the coordinates transformed by the twin operator are equally valid. Structural figures were created using the program PyMOL (Available at: http://www.pymol.org).

## RESULTS AND DISCUSSION

In this study, we were able to determine the complete structure of 15*S*-LOX1 by reinterpreting the reported X-ray data in the R3 space group [Fig. 1(c)]. The final model contains the entire 1324 residues for two molecules (residues 2–663), an inhibitor (3-(2-octylphenyl)-propanoic acid), and 219 water molecules. The geometry of the final model is good with three residues in the generously allowed regions and no residue in the disallowed regions in the Ramachandran plot.[29] The final $2F_o - F_c$ electron density map is well-resolved and relatively clean, as shown in Figure 1(d) for the two α2 helices. The general aspects of LOX structure as well as the structural characteristics of regulatory N-terminal β-barrel are not described here, as they are well discussed or reviewed in the previous articles.[7,12,13,17]

### Comparison of the two 15S-LOX1 structures

The crystal of 15*S*-LOX1 is interesting in that it has two proteins in the asymmetric unit, one with inhibitor and the other without, existing in two distinct forms. The molecule with inhibitor assumes the closed form in which the access to the binding pocket is blocked by α2. The ligand-free molecule assumes the open form in which the entrance is wide open but the pocket is shallow. These suggest that 15*S*-LOX1 may undergo ligand-induced conformation changes. The two molecules are related by pseudo-twofold axis that is virtually coincident with the crystallographic twofold axis in R32. The dimer interface formed by the two α2 helices mainly consists of hydrophobic interactions without any hydrogen bond [Fig. 1(d)].

The two R3 structures and the R32 structure are superposed in Figure 1(e) and the Cα···Cα distances between the equivalent residues are plotted in Figure 1(f). The original R32 structure with inhibitor is more similar to the open form without inhibitor. It shows *rms* deviations of 0.49 Å for the 625 Cα atoms and 0.47 Å for the 641 Cα atoms with the open and closed forms, respectively. All residues missing in the R32 model belong to the regions where the two R3 forms are structurally different (see below). The electron densities for these regions are absent, poorly resolved or broad in the map calculated from the original R32 model whereas they are clearly defined in the map of the current R3 model. The R32 structure was modeled incorrectly at several places including, for instance, Gln596 and Leu597 which are critical in defining the substrate-binding cavity.

For the two R3 structures, the equivalent Cα atoms of the 619 residues (94% of 662) are related by pseudo-twofold symmetry with an *rms* deviation of 0.59 Å. The remaining Cα atoms deviate from the pseudo-symmetry by distances ranging from 2.4 to 16.0 Å. Major structural differences are found in the three spatially adjacent segments. These include residues 167−199 (labeled as I), 205−215 (II), and 592−604 (III). Segment I of 33 residues, including α2, shows the largest difference with the maximum Cα···Cα distance of 16.0 Å for Asn190. The


DOI 10.1002/prot

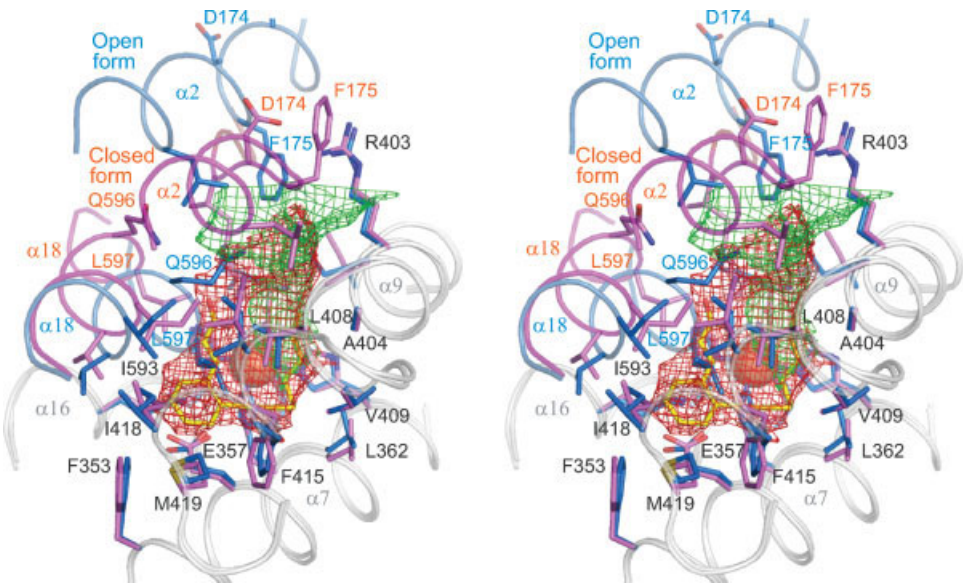


**Figure 2**

*Comparison of the substrate-binding cavities in the open and closed forms of 15S-LOX1 (in stereoview). The secondary structural elements and the selected residues in both forms are superposed together with the cavities depicted as meshes, which are colored in green and red for the open and closed forms, respectively. The iron and the ligating ligand residues are shown behind the meshes. Note that the side chain of Leu597 in the open form partly overlays with the inhibitor (yellow stick) in the closed form.*

two α2 helices are separated by ∼12 Å. They differ in helical length; the open form has seven turns (Leu168-Ile194) while the closed form has five turns (Phe175-Asn193). With regard to this segment, therefore, the conformational change from the open to closed form can be envisaged to occur by unfolding residues Phe167-Asp174 and extending the chain of Asn193-Lys199 and thereby swinging α2 toward the open space.

The conformational differences of segments II and III are correlated with that of segment I. Segment III comprising 13 residues contains the C-terminal end of α18 (Ile593-Gly598), which lies beneath α2 and is critical in shaping the substrate-binding cavity, and the following chain of six residues (Arg599-Ile603). In the closed form, this segment is displaced by ∼6 Å from its position in the open form because of the movement of Glu169-Phe175 in segment I toward it. This displacement, in turn, induces a change in the loop structure of segment II comprising 11 residues. Otherwise, Trp595 in segment III would collide with Cys210 in segment II.

## Comparison of the substrate-binding cavities

Both R3 forms markedly differ in the shape of their substrate-binding cavities, as shown in Figure 2. In this figure, the cavity is represented by the solvent accessible surface built with a probe size of 1.8 Å to depict the space available for the hydrophobic lipid molecule. In the open form, the cavity is funnel shaped, wide open to the protein surface, and its inside is shallow and narrow. In the closed form, the cavity is deep and wide and is isolated from the protein surface. Leu597 located at the C-terminal turn of α18 is a crucial determinant for controlling the shape and size of the cavity. In the open form, the side chain of Leu597 protrudes into the cavity defining one side of its bottom; it occupies the same space as the propanoic acid moiety of the inhibitor in the closed form. In the closed form, the segment containing Leu597 retreats from the cavity, opening the inner space to the inhibitor. Concurrently, the α2 helix closes the entry to the cavity making it inaccessible from the surface. The Cα atoms of Leu597 in both forms are separated by 5.8 Å. It is worthy to note that, in soybean LOX-L3, the corresponding residue Leu773 was pinpointed as crucial for its stereospecificity.[14]

The binding cavity of the closed form appears like a bowed thick sheet that is concaved by the side chain of Leu408. Leu408 is on the seven residue-long loop connecting α9–α10. The structure of this loop is conserved in all known LOXs. The cavity is formed mainly by the side chains of 23 amino acid residues from six helices and a loop. They include Ile173, Phe175, and Ser178 on α2; Phe353, Glu357, His361, Leu362, and His366 on α7; Ile400, Arg403, and Ala404 on α9; Leu408 and Val409 on the α9-α10 loop; Ile414, Phe415, Ile418, and Met419 on α10; His545 and Gln548 on α16; and Ile593, Val594, Gln596, and Leu597 on α18. In addition, the main chain

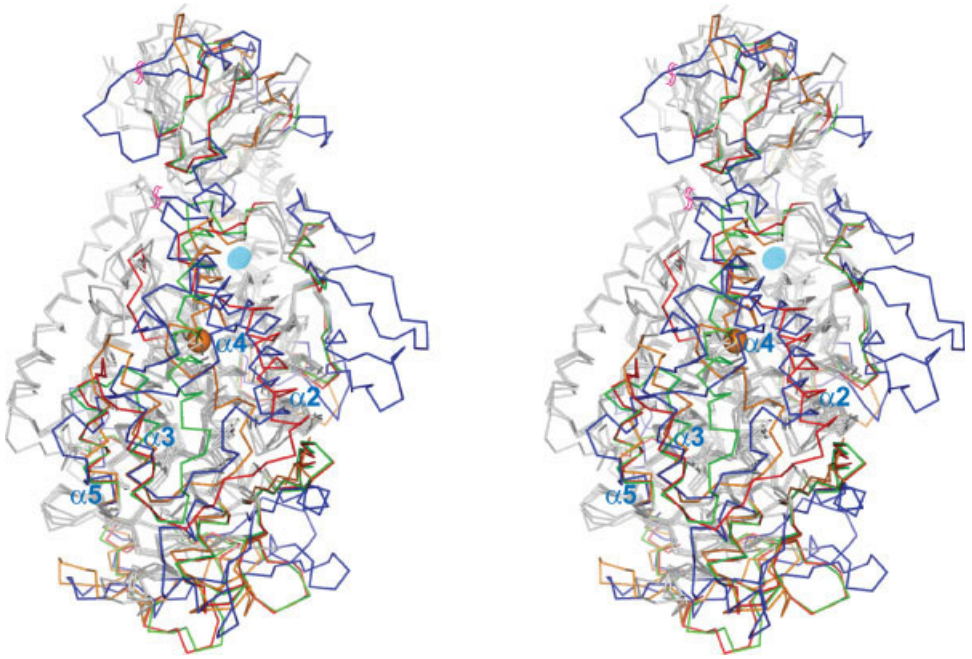


**Figure 3**

*Comparison of the three LOX crystal structures (in stereoview). Cα-traces of the open and closed forms of 15S-LOX1, coral 8R-LOX, and soybean LOX-L3 are superposed and colored in green, red, orange, and blue, respectively, for the regions that markedly differ from each other. For LOX-L3, 13 residues between two wavy magenta marks in the N-terminal domain are disordered. The labels of the α helices are those for LOX-L3 and the small disk in cyan represents the plausible entry to its cavity.*

atoms of Asp174, Leu179, Gly407, and Ile663 are in contact with the cavity. Among the residues in the cavity, His361, His366, His545, and Ile663 are the iron-ligating residues. The inhibitor with a planar structure fits well into the bottom half of the cavity. Its carboxylate moiety points toward the iron; however, the Fe—O distance (5.3 Å) in the present structure is longer than that (3.8 Å) in the R32 structure.

It should be emphasized that, in the R32 structure, several residues at the C-terminal region of α18 were modeled, accommodating the inhibitor, similar to those in the closed form, while the disconnected α2 was modeled like α2 in the open form. If the α2 were modeled completely, a clash could have occurred between Leu179 at α2 and Gln596 at α18; residue Leu179 and the side chain of Gln596 are absent in that model.

## Comparison with other LOX structures

The structures of rabbit 15*S*-LOX1 are superposed with those of soybean LOX-L3[11] and coral 8*R*-LOX[13] in Figure 3. 15*S*-LOX1 (662 residues) shares higher sequence identity with 8*R*-LOX (693 residues, 28.7%) than with LOX-L3 (857 residues, 19.7%), and is more similar to 8*R*-LOX than LOX-L3 in the overall structure. LOX-L3 has more extended surface loops than the others have. The open and closed forms of 15*S*-LOX1 overlay with the structure of 8*R*-LOX with *rms* deviations of 1.52 Å for the 580 Cα atoms and 1.60 Å for the 578 Cα atoms, respectively.

By comparing the structure of 8-*R*LOX and the R32 structure of 15*S*-LOX1, Oldham *et al.* indicated that the placement of the elements of secondary structure are strikingly conserved at the "lower" half of the catalytic domain but there is deviation in the positions of the shorter helices at its entrance side.[13] We also noticed that the long segments that form the "upper" half of the catalytic domain and may determine the site of the entry to the cavity show significant structural variations in the three proteins. They include 69 residues (Lys157-Glu225) in 15*S*-LOX1, 69 residues (Thr161-Glu229) in 8*R*-LOX, and 105 residues (Val256-Thr360) in LOX-L3. In 15*S*-LOX1 and 8*R*-LOX, these segments have the common loop-α2-loop-α3-loop-α4 topology, but their structures are considerably different being observed in three distinct conformational states. For the Cα atoms of these segments, 8*R*-LOX shows *rms* deviations of 4.28 Å and 7.02 Å with the open and closed form of 15*S*-LOX1, respectively. In 8*R*-LOX, α2 was broken into three short helices angled to one another.[13] These structural variations are indicative of a considerable degree of conformational flexibility present in this region of animal LOXs.

In contrast, soybean LOX-L3 seems to have a compact and rigid structure in this region, although it shows


DOI 10.1002/prot

greater flexibility than the core region indicated by large temperature factors and not well defined electron density.[11] LOX-L3 has an extra loop-α4-loop structure of 36 residues (Tyr311-Pro346) intervening between α3 and α5, which overlay α3 and α4 in 15*S*-LOX1, respectively. Thus, unlike α2 in animal LOXs, any helix in this segment may have no room for large movements. In support of this notion, LOX-L3 showed no major structural change upon ligand binding.[14–18] Superposition of a free and six liganded LOX-L3 structures shows that the chain of Leu331-Gln341 juxtaposing α4 made the largest movement but by only 3 Å. α2 in the open form of 15*S*-LOX1 is situated beneath α4 of LOX-L3, whereas that in the closed form overlays α2 of LOX-L3. In 8*R*-LOX, a short helix partly overlays α2 of LOX-L3 and the other is situated beneath α4. As far as the movement of α2 is concerned, therefore, it appears that both forms of 15*S*-LOX1 represent two extreme conformations while 8*R*-LOX represents an intermediate state.

In LOX-L3, the substrate-binding cavity has an elongated boot shape. The site of entry to the cavity appears to be different from that in 15*S*-LOX1 because of compact packing around α2. A putative site could be found in a loop region preceding α2 as shown in Figure 3. In soybean LOX, changes in cavity size and shape can be done within the cavity by rearranging side chains and the main chain to much lesser degree,[20] while much more extensive changes including movements of a long helix and reorientation of several residues in the 'hinges' are observed in 15*S*-LOX1 (Fig. 2). Ligand-free 8*R*-LOX has two well-resolved internal cavities.[13] A constriction was formed by Leu386 and Leu628, which are equivalent to Leu362 (on α7) and Leu597 (on α18) of 15*S*-LOX1, respectively. Neither of the cavities has clear access to the surface. The cavity in 8*R*-LOX is deeper by ~4.7 Å than that in the closed form of 15*S*-LOX1, the depths being defined mainly by Ser377 and Phe353, respectively. Its width is narrower as Leu432 was shifted by ~2 Å toward the catalytic iron compared to the equivalent Leu408 of 15*S*-LOX1. Oldham *et al.* proposed that, when 8*R*-LOX binds a substrate, the movement of Trp179 (equivalent to Phe175 on α2 of 15*S*-LOX1) may be required to gain access to the cavity and a rotamer change of Leu386 and a shift of Leu628 to open up the constriction.[13] We now propose that, upon ligand binding, 8*R*-LOX may also undergo major conformational changes larger than local movements as in the case of 15*S*-LOX1.

## SUMMARY

In this study, we have reinterpreted the crystal structure of 15S-LOX1 based on the data deposited in PDB as 1lox in 1997 by Gillmor *et al.*[12] We have refined the original structure as two independent molecules in the space group R3, assuming that the crystal used for their study, reported as space group R32, was a twin. In the new model, there is no crystal packing problem and the "disordered" α2 helix is well resolved in the two distinct conformations. It should be noted that the final molecular structures obtained from the R3 twin model could be comparably refined using the disorder model in R32 (see Appendix). However, the model building in this case would have been impractical because of the unresolved map where the densities of the disordered conformers would overlap each other. The revised structure suggests that large conformational changes may occur in mammalian LOX upon ligand binding. The regions incorrectly determined in the original structure are limited to a small portion of the whole structure, leaving the global view for LOX structure unchanged. However, these regions are functionally important as they include the residues that form the entrance side of the substrate-binding cavity. The R3 structure, especially the closed form, may provide new insight about the arachidonate binding to mammalian LOXs.

The two distinct forms of 15*S*-LOX1 helped us delineate the following dynamic events that may plausibly occur during the catalytic reaction. Initially, the substrate sticks into the shallow cavity through the wide-open entrance in the open form. As it penetrates into the cavity, segment III containing Leu597 is pushed toward the protein surface, enlarging the cavity. The movement of this inner segment forces nearby outer segments I and II to move outward. Segments I undergoes large conformational changes such that α2 partially unwinds and moves to close the entrance becoming a closed form. The reverse sequence of movements may occur upon product release. The dynamic nature of α2 may have another functional importance, because it bears Trp181, one of the residues that are implicated to be important in calcium-dependent membrane binding of 15*S*-LOX1.[30] Trp181 is positioned toward the protein surface in both forms. The flexibility in animal LOXs may be one of the features differentiating them from plant LOXs.

The elucidation of association mode between LOX and arachidonic acid is important in understanding the origin of regio- and stereospecificity of a specific LOX. As the crystal structure for the complex is not available yet, this has been done by modeling studies. There are several complex models for 15*S*-LOX1 made using the structure of soybean LOX or the R32 model.[17,30–33] A complex model for 8*R*-LOX was also reported recently.[13] In these models, the arachidonate has been depicted as assuming an elongated boot form bound in the methyl end-first orientation. The present study shows that an alternative complex model can be considered since the closed form of 15*S*-LOX1 represents a new structure for LOX. Its cavity shape suggests that the arachidonate may bind in the horseshoe-like conformation. However, it remains to be determined whether the closed form is truly a productive form. From the structures of 15*S*-LOX1 and 8-*R*LOX, we

found that, in addition to the outer α2, the inner α7, and α9-loop-α10 as well as α18 also show significant deviations, albeit to a much lesser extent than α2, in their positions. These structures indicate that the cavity wall close to the catalytic iron may be somewhat rigid, but the other side of the cavity may be flexible enough to adjust its shape to the ligand structure, as previously noted in the comparative studies of the soybean LOX structures.[20] Knowledge on the conformational flexibility of mammalian LOXs may be helpful for further studies on site-directed mutagenesis and structure-based inhibitor design.

## ACKNOWLEDGMENTS

The authors are grateful to the anonymous referees for their careful reading of the manuscript and for their valuable comments. JC was a recipient of the BK21 fellowship.

## REFERENCES

1. Brash AR. Lipoxygenases: occurrence, functions, catalysis, and acquisition of substrate. J Biol Chem 1999;274:23679–23682.
2. Kühn H, Thiele BJ. The diversity of the lipoxygenase family. Many sequence data but little information on biological significance. FEBS Lett 1999;449:7–11.
3. Oliw EH. Plant and fungal lipoxygenases. Prostaglandins Other Lipid Mediat 2002;68/69:313–323.
4. Liavonchanka A, Feussner I. Lipoxygenases: occurrence, functions and catalysis. J Plant Physiol 2006;163:348–357.
5. Funk CD. Prostaglandins and leukotrienes: advances in eicosanoid biology. Science 2001;294:1871–1875.
6. Samuelsson B, Dahlen SE, Lindgren JA, Rouzer CA, Serhan CN. Leukotrienes and lipoxins: structures, biosynthesis, and biological effects. Science 1987;237:1171–1176.
7. Kühn H, Walther M, Kuban RJ. Mammalian arachidonate 15-lipoxygenases structure, function, and biological implications. Prostaglandins Other Lipid Mediat 2002;68/69:263–290.
8. Serhan CN. Clues for new therapeutics in osteoporosis and periodontal disease: new roles for lipoxygenases? Expert Opin Ther Targets 2004;8:643–652.
9. Hamerman D. Osteoporosis and atherosclerosis: biological linkages and the emergence of dual-purpose therapies. QJM 2005;98:467–484.
10. Minor W, Steczko J, Stec B, Otwinowski Z, Bolin JT, Walter R, Axelrod B. Crystal structure of soybean lipoxygenase L-1 at 1.4 Å resolution. Biochemistry 1996;35:10687–10701.
11. Skrzypczak-Jankun E, Amzel LM, Kroa BA, Funk MO, Jr. Structure of soybean lipoxygenase L3 and a comparison with its L1 isoenzyme. Proteins 1997;29:15–31.
12. Gillmor SA, Villasenor A, Fletterick R, Sigal E, Browner MF. The structure of mammalian 15-lipoxygenase reveals similarity to the lipases and the determinants of substrate specificity. Nat Struct Biol 1997;4:1003–1009.
13. Oldham ML, Brash AR, Newcomer ME. Insights from the X-ray crystal structure of coral 8R-lipoxygenase: calcium activation via a C2-like domain and a structural basis of product chirality. J Biol Chem 2005;280:39545–39552.
14. Skrzypczak-Jankun E, Bross RA, Carroll RT, Dunham WR, Funk MO, Jr. Three-dimensional structure of a purple lipoxygenase. J Am Chem Soc 2001;123:10814–10820.
15. Skrzypczak-Jankun E, Zhou K, McCabe NP, Selman SH, Jankun J. Structure of curcumin in complex with lipoxygenase and its significance in cancer. Int J Mol Med 2003;12:17–24.
16. Skrzypczak-Jankun E, Zhou K, Jankun J. Inhibition of lipoxygenase by (−)-epigallo-catechin gallate: X-ray analysis at 2.1 Å reveals degradation of EGCG and shows soybean LOX-3 complex with EGC instead. Int J Mol Med 2003;12:415–420.
17. Borbulevych OY, Jankun J, Selman SH, Skrzypczak-Jankun E. Lipoxygenase interactions with natural flavonoid, quercetin, reveal a complex with protocatechuic acid in its X-ray structure at 2.1 Å resolution. Proteins 2004;54:13–19.
18. Skrzypczak-Jankun E, Borbulevych OY, Jankun J. Soybean lipoxygenase-3 in complex with 4-nitrocatechol. Acta Crystallogr D Biol Crystallogr 2004;60:613–615.
19. Kühn H, Saam J, Eibach S, Holzhütter HG, Ivanov I, Walther M. Structural biology of mammalian lipoxygenases: enzymatic consequences of targeted alterations of the protein structure. Biochem Biophys Res Commun 2005;338:93–101.
20. Skrzypczak-Jankun E, Borbulevych OY, Zavodszky MI, Baranski MR, Padmanabhan K, Petricek V, Jankun J. Effect of crystal freezing and small-molecule binding on internal cavity size in a large protein: X-ray and docking studies of lipoxygenase at ambient and low temperature at 2.0 Å resolution. Acta Crystallogr D Biol Crystallogr 2006;62:766–775.
21. Borngräber S, Browner M, Gillmor S, Gerth C, Anton M, Fletterick R, Kühn H. Shape and specificity in mammalian 15-lipoxygenase active site. The functional interplay of sequence determinants for the reaction specificity. J Biol Chem 1999;274:37345–37350.
22. Kühn H. Structural basis for the positional specificity of lipoxygenases. Prostaglandins Other Lipid Mediat 2000;62:255–270.
23. Coffa G, Schneider C, Brash AR. A comprehensive model of positional and stereo control in lipoxygenases. Biochem Biophys Res Commun 2005;338:87–92.
24. Charlier C, Hénichart JP, Durant F, Wouters J. Structural insights into human 5-lipoxygenase inhibition: combined ligand-based and target-based approach. J Med Chem 2006;49:186–195.
25. Kenyon V, Chorny I, Carvajal WJ, Holman TR, Jacobson MP. Novel human lipoxygenase inhibitors discovered using virtual screening with homology models. J Med Chem 2006;49:1356–1363.
26. Brünger AT, Adams PD, Clore GM, DeLano WL, Gros P, Grosse-Kunstleve RW, Jiang JS, Kuszewski J, Nilges M, Pannu NS, Read RJ, Rice LM, Simonson T, Warren GL. Crystallography and NMR system: a new software suite for macromolecular structure determination. Acta Crystallogr D Biol Crystallogr 1998;54:905–921.
27. Jones TA, Zou JY, Cowan SW, Kjeldgaard M. Improved methods for building protein models in electron density maps and the location of errors in these models. Acta Crystallogr A Found Crystallogr 1991;47:110–119.
28. Collaborative Computational Project, Number 4. The CCP4 suite: programs for protein crystallography. Acta Crystallogr D Biol Crystallogr 1994;50:760–763.
29. Laskowski RA, MacArthur MW, Moss DS, Thornton JM. PROCHECK: a program to check the stereochemical quality of protein structures. J Appl Crystallogr 1993;26:283–291.
30. Walther M, Wiesner R, Kühn H. Investigations into calcium-dependent membrane association of 15-lipoxygenase-1. Mechanistic roles of surface-exposed hydrophobic amino acids and calcium. J Biol Chem 2004;279:3717–3725.
31. Gan QF, Browner MF, Sloane DL, Sigal E. Defining the arachidonic acid binding site of human 15-lipoxygenase. Molecular modeling and mutagenesis. J Biol Chem 1996;271:25412–25418.
32. Borngräber S, Browner M, Gillmor S, Gerth C, Anton M, Fletterick R, Kühn H. Shape and specificity in mammalian 15-lipoxygenase active site. The functional interplay of sequence determinants for the reaction specificity. J Biol Chem 1999;274:37345–37350.
33. Romanov S, Wiesner R, Myagkova G, Kühn H, Ivanov I. Affinity labeling of the rabbit 12/15-lipoxygenase using azido derivatives of arachidonic acid. Biochemistry 2006;45:3554–3562.
34. Chandra N, Acharya KR, Moody PC. Analysis and characterization of data from twinned crystals. Acta Crystallogr D Biol Crystallogr 1999;55:1750–1758.

 DOI 10.1002/prot

35. Contreras-Martel C, Martinez-Oyanedel J, Bunster M, Legrand P, Piras C, Vernede X, Fontecilla-Camps JC. Crystallization and 2.2 Å resolution structure of R-phycoerythrin from Gracilaria chilensis: a case of perfect hemihedral twinning. Acta Crystallogr D Biol Crystallogr 2001;57:52–60.
36. Lebedev AA, Vaqin AA, Murshudov GN. Intensity statistics in twinned crystals with examples from the PDB. Acta Crystallogr D Biol Crystallogr 2006;62:83–95.
37. Britton D. Estimation of twinning parameter for twins with exactly superimposed reciprocal lattices. Acta Crystallogr A 1972;28:296–297.
38. Yeates TO. Detecting and overcoming crystal twinning. Methods Enzymol 1997;276:344–358.

## APPENDIX

As described in the Crystallographic analysis section, the two conformers should be packed against each other to avoid bumping. This inevitably removed the crystallographic twofold symmetry, shifting the space group of the unit-cell from R32 to R3. However, Gillmor *et al.* reported rather a small value (0.073) of $R_{sym}$, the residual of averaging symmetry-equivalent reflection intensities for R32.[12] To resolve this apparent discrepancy we have developed several alternative hypotheses:

1. The unit-cells that had R3 symmetry locally were packed together in a disordered fashion, and thus the crystal as a whole was in R32 space group (R32 disorder model). In other words, the R3 unit-cell and the one related by twofold shared the same lattice dimensions, and thus might have been packed together to form a coherently diffracting crystal. It should be noted that there were two potential modes of disordering. In one case, only the helix might have been disordered and the rest of the molecule obeyed the R32 symmetry (Case 1). In the other case, the whole molecule might have departed from the R32 symmetry by a noticeable amount (Case 2).
2. The R3 unit-cells mentioned above were packed regularly to form a crystal in R3 space group. In this case most part of the molecules obeyed R32 crystallographic twofold symmetry except for the α2 helices that deviated from the R32 symmetry. As their contribution to the structure factors was much less than that of the rest of the molecule, the resulting $R_{sym}$ might have looked like that of R32. This would be similar to the R32 disorder model Case 1 in terms of various statistics and would require high resolution data to resolve. For the current data, we would not consider this model separately. Instead, we considered a model where the R3 micro-crystals just described might have been packed in such a way that formed a twinned macro-crystal (R3 twin model). In this case, homogeneous R3 micro-crystals might have grown independently but twinned because of the compatibility of their lattices. This twinning might have introduced twofold symmetry in observed diffraction pattern and resulted in such a low $R_{sym}$.

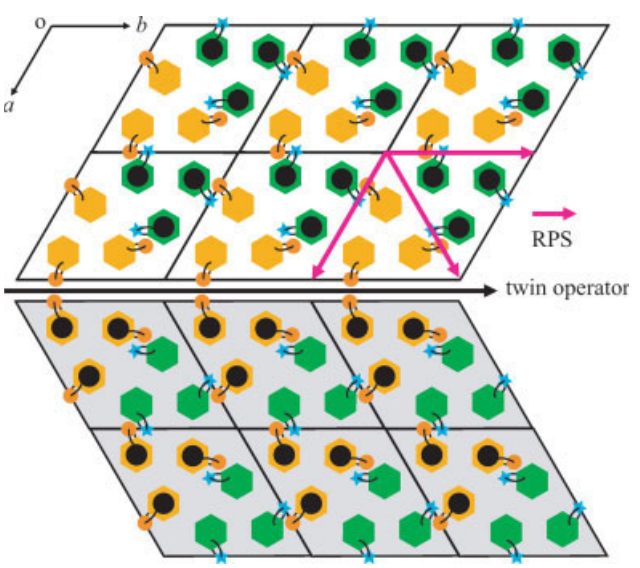


**Figure 4**

*Schematic representation of a perfect hemihedral twin with coinciding RPS in R3 (hexagonal axes). Each protein molecule is represented by a filled hexagon. A 'green' hexagon is related to an 'orange' one by the RPS operator that is virtually parallel to* a, b, *or* a + b. *The features distinguishing these two molecules (the "disordered" α helices in 15S-LOX1) are signified by the matching small disk and star. The black disk within the hexagon is to denote the orientation along the c-axis: the molecules with and without the disk facing up and down, respectively, and vice versa. The molecules related by rhombohedral centering are omitted for clarity.*

In the R3 twin case, the observed intensity would be the sum of contributions from the component crystallites, while in the R32 disorder case the structure factor, not the intensity, would be the vector sum of the individual contributions. As such, the refinement and model building in R3 twin case would be much more straightforward than working with R32 disorder models. It is also well known that R3 crystals are prone to be twinned.[34,35] Recently, Lebedev *et al.* analyzed the published structures in PDB, and found that R3 crystals have been occasionally mistaken as R32 especially when twinning occurred in association with rotational pseudo-symmetry (RPS) parallel to the twinning operator (refer to Fig. 4).[36] In R3 space group, *a*, *b*, and *a* + *b* can be twin operators. The issue of twinning potentially interfering with RPS could be very complicated; it could not be easily resolved by the usual statistical twinning tests that are typically tested prior to structure determination.[37,38] Lebedev *et al.* suggested a set of tests that could be useful in this case.[36] They defined $R_{twin}$, the residual difference between intensities of the **h** and **h**′ reflections related by the twin operator:

$$R_{twin} = \sum \left| I_{\mathbf{h}} - I_{\mathbf{h}'} \right| \Big/ \sum \left| I_{\mathbf{h}} + I_{\mathbf{h}'} \right| \qquad (1)$$

where $I_{\mathbf{h}}$ and $I_{\mathbf{h}'}$ can be based on either $F_{obs}$ or $F_{calc}$. They showed that the expected value of $R_{twin}$(obs)

approaches zero for perfect twin crystals, while $R_{twin}$(obs) becomes approximately equal to $R_{twin}$(calc) for untwinned normal crystals and becomes smaller than $R_{twin}$(calc) for partially twinned crystals. When RPS interferes with twinning, a correlation between observations related by twinning operators could be caused either by RPS or by both RPS and twinning. The two cases cannot be discriminated by $R_{twin}$(obs) alone, for which cases twinning detection prior to the structure determination is particularly difficult. Lebedev *et al.* showed that the expected value of $R_{twin}$(calc) approaches 0.5 when there is no RPS, but becomes smaller than 0.5 when RPS is present.[36] Thus, after the structure refinement is completed, the analysis of $R_{twin}$'s serves as a diagnostic tool to check whether the current hypothesis on the presence of twinning and pseudo-twofold symmetry is reasonable or not.

The structure factors for 15S-LOX1 were available from PDB in a form that had been merged in R32. On the basis of the previously reported $R_{sym}$, it was possible to estimate $R_{twin}$(obs) without the unmerged structure factor values. Whereas $R_{twin}$ is concerned with the difference between $I(hkl)$ and $I(kh-l)$, $R_{sym}$ considers other crystallographic symmetries as well. It can be shown that $R_{twin}(\text{obs}) \leq R_{sym}$ and becomes equivalent to $R_{sym}$ if there is no experimental error (e.g., the reflection intensities related by threefold symmetry are exactly the same). Therefore, low $R_{sym}$ guarantees low $R_{twin}$(obs). Having established that $R_{twin}$(obs) might have been close to zero, we then needed $R_{twin}$(calc). If $R_{twin}$(calc) also turned out to be very small, it would be likely that the crystals of 15*S*-LOX1 might have been untwinned in R32 (R32 disorder model Case 1). The two molecules should then be identical except in the "disordered" α2 helical region where each molecule would adopt its own conformation. As they had to be related by the crystallographic twofold axis, we should model them with static disorder. To test that this was indeed the case, we needed $R_{twin}$ (calc) from the refined model in R3 space group. The two molecules should be allowed to move independently throughout the refinement. Otherwise, the restriction of R32 is inevitably imposed and the resulting $R_{twin}$(calc) would be close to zero.

We carried out the refinement using CNS with the perfect hemihedral twin option in R3. In this option, CNS tries to fit $sqrt(|F_{calc}(hkl)|^2 + |F_{calc}(kh-l)|^2)$ to $F_{obs}(hkl)$, where $F_{obs}(hkl)$ should be calculated from the reflection intensity that had been averaged over the twin operator.[26] As noted earlier, the $F_{obs}$ values downloaded from PDB had been processed in R32 and were used as they were. Refinement via simulated annealing with interspersed manual model revision proceeded as usual and converged to a stage where the residuals were slightly better than the original values with comparable geometrical *rms*. $R_{twin}$(calc) based on the final model was 0.210. This value is undoubtedly larger than $R_{twin}$(obs), consistent with the presence of crystal twinning. It is also substantially lower than 0.5, indicating the presence of RPS. In our final model, the pseudo-twofold axis relating the two molecules slightly deviated from the twin axis by 0.07 Å and 0.23 Å, and the *rms* deviations between the equivalent Cα atoms except for the α2 helices was 0.59 Å. All these results favored the perfect twin model in R3 (R3 twin model) over that of the static disorder model of the α2 helix in R32 (Case 1). However, it should be noted that the final molecular structures obtained from the R3 twin model could have been comparably refined in the R32 disorder model (Case 2). Although the model building in the latter case would have been impractical because of the unresolved map where the densities of the disordered conformers would overlap each other, the refinement and R-factor calculation could have been done using the final structures of the R3 twin model. The difference between these two models was in the issue whether one had to average the structure factors in complex numbers or just the intensities; it would not be trivial to differentiate them at moderate resolutions as in this case and would require high resolution data.


DOI 10.1002/prot